AIP | Journal of Applied Physics

Cation composition effects on electronic structures of In-Sn-Zn-O amorphous semiconductors

Ji-Young Noh, Hanchul Kim, Ho-Hyun Nahm, Yong-Sung Kim, Dae Hwan Kim et al.

Citation: J. Appl. Phys. **113**, 183706 (2013); doi: 10.1063/1.4803706
View online: http://dx.doi.org/10.1063/1.4803706
View Table of Contents: http://jap.aip.org/resource/1/JAPIAU/v113/i18
Published by the AIP Publishing LLC.

Additional information on J. Appl. Phys.

Journal Homepage: http://jap.aip.org/
Journal Information: http://jap.aip.org/about/about_the_journal
Top downloads: http://jap.aip.org/features/most_downloaded
Information for Authors: http://jap.aip.org/authors

ADVERTISEMENT

Downloaded 29 Aug 2013 to 210.123.42.185. This article is copyrighted as indicated in the abstract. Reuse of AIP content is subject to the terms at: http://jap.aip.org/about/rights_and_permissions

JOURNAL OF APPLIED PHYSICS **113**, 183706 (2013)

Cation composition effects on electronic structures of In-Sn-Zn-O amorphous semiconductors

Ji-Young Noh,[1,2] Hanchul Kim,[1] Ho-Hyun Nahm,[2] Yong-Sung Kim,[2,3,a)] Dae Hwan Kim,[4] Byung-Du Ahn,[5] Jun-Hyung Lim,[5] Gun Hee Kim,[5] Je-Hun Lee,[5] and Junho Song[5]
[1]*Department of Physics, Sookmyung Women's University, Seoul 140-742, South Korea*
[2]*Korea Research Institute of Standards and Science, Daejeon 305-340, South Korea*
[3]*Department of Nano Science, University of Science and Technology, Daejeon 305-350, South Korea*
[4]*School of Electrical Engineering, Kookmin University, Seoul 136-702, South Korea*
[5]*Samsung Display Co., Ltd., Yongin 446-711, South Korea*

(Received 11 January 2013; accepted 16 April 2013; published online 9 May 2013)

Based on density-functional theory calculations, the effects of cation compositions on electronic structures of In-Sn-Zn-O amorphous semiconductors were investigated. We considered various composition ratios of In, Sn, and Zn in O stoichiometric condition, and found that the conduction band minimum (CBM) energy level decreases and the valence band tail (VBT) energy level extent increases as the sum of In and Sn ratios ($R_{In}+R_{Sn}$) increases. The CBM lowering is attributed to the increased overlap of the In-5*s* and Sn-5*s* orbitals as the $R_{In}+R_{Sn}$ increases, and correspondingly the electron effective masses (m_e^*) are found to be reduced. The VBT increase is found to be due to the increased density of the In and Sn atoms, near which the O-2*p* inter-site $pp\sigma^*$ coupling is larger than that near the Zn atoms. The acute O-(In,Sn)-O angles are suggested to be structurally important, giving the stronger O-O $pp\sigma^*$ coupling. © *2013 AIP Publishing LLC*. [http://dx.doi.org/10.1063/1.4803706]

I. INTRODUCTION

Amorphous oxide semiconductors (AOS) have high electron mobility (>10 $cm^2\ V^{-1}\ s^{-1}$) even in the amorphous phase.[1] The amorphous $InGaZnO_4$ is a prototype AOS, and various kinds of AOS with alternative cations (Sn, Hf, Zr, Al, Si, and so on) have been suggested.[2–6] Basically, the high electron mobility originates from the cation *s*-like orbitals of the conduction band (CB) states. Since the *s* orbitals are spherical, their inter-site overlap is robust to the orientational disorder of the amorphous structure.[7] It is in stark contrast to the hydrogenated amorphous Si (a-Si:H), which has the sp^3-hybridized conduction bands and exhibits severe localization of the sp^3 orbitals in amorphous phase (giving the conduction band tail states). Thus, the electron mobility of a-Si:H is degraded to about ~1 $cm^2\ V^{-1}\ s^{-1}$ from that of the crystalline Si of about ~200 $cm^2\ V^{-1}\ s^{-1}$.

With the high mobility, the AOS has process compatibility. The low (room) temperature thin-film deposition process (usually sputtering) makes it possible to manufacture large-area thin-films on a variety choice of substrates, such as soda-lime glasses and flexible organic plastics, with low-cost and a high production (deposition) rate.[8,9] Electronics on a large-area transparent substrate for commercial flat-panel displays have used a-Si:H thin-film transistors (TFTs), and large-area low-cost solar cells have been made by using a-Si:H *pn* junctions. The requirement of high speed TFTs for the next-generation high-resolution larger-area flat-panel displays makes the use of a-Si:H TFTs doubted due to its fundamental limit of electron mobility, and a new way by utilizing the AOS-based TFTs is nowadays intensively pursued.[10]

However, the facing bottleneck of the AOS-based TFTs for display applications is their instabilities under bias and/or illumination stress (IS). By positive gate-bias stress (PBS) in AOS-based TFTs, the threshold voltage (V_{th}) of the TFTs is known to be positive-shifted,[11–17] and by negative bias and illumination stress (NBIS)[4,5,17–24] or only by IS,[17,25–29] the V_{th} is largely negative-shifted. The NBIS is known to be the most serious among the stresses,[18] and it is important in active matrix liquid crystal displays (AM-LCD), since it is applied to the TFTs in AM-LCD steadily in the normal off-state stand-by condition. On the other hand, the PBS is steadily applied to the TFTs in active matrix organic light emitting diode (AM-OLED) displays during the normal state.

Understanding the microscopic mechanisms of the instabilities in AOS-based TFTs has been recently advanced. For the PBS instability, (i) it has been suggested that the electrons attracted to the gate electrode are trapped at the interface between the AOS channel and the gate insulator and/or injected into the gate insulator.[11–13,17] (ii) The electron traps at H_2O-related trap sites have been also suggested.[14] The electron traps can make a positive-shift of the V_{th} electrostatically, but their meta-stability is not clear yet. (iii) Surface doping induced by O_2 and H_2O molecules has been suggested as another mechanism.[15] (iv) More importantly, it has been proposed that acceptor-like deep states is generated in AOS by the PBS.[16] For the NBIS and IS instabilities, a few plausible models have been suggested. (i) Holes are generated by the light illumination and trapped at the interface and/or injected into the gate insulator.[4,22,23] However, the IS instability has been observed not only in AOS TFTs but also in AOS thin films without a gate insulator through persistent photo-conductivity (PPC),[26,29] and thus there has been considered to be an intrinsic mechanism in AOS materials.[22,26]

a)yongsung.kim@kriss.re.kr

 © 2013 AIP Publishing LLC

Downloaded 29 Aug 2013 to 210.123.42.185. This article is copyrighted as indicated in the abstract. Reuse of AIP content is subject to the terms at: http://jap.aip.org/about/rights_and_permissions

(ii) NBIS or IS desorbs surface O atoms (reduction) and accordingly dope electrons,[5] and an overlying passivation layer on AOS TFTs has been adopted to avoid it.[5] Although somewhat improved, the NBIS and IS instabilities have been still serious even with avoiding the surface effect.[4,19,20,22] (iii) Photo-ionized O-vacancies (V_O) persist with slow electron recombination.[19–22,24,30,31] The V_O can give photo-carriers and be a hole-trap, but the meta-stability of the ionized V_O remains unclear. The recovery time of the negative-shifted V_{th} in AOS TFTs[19,26–28] and the persistency of the PPC in AOS thin films[26,29] are an order of days at room temperature, and the energy barrier from the meta-stable to the stable state should be very high. The activation energy has been reported to be in the range of 0.9–1.0 eV experimentally.[29] (iv) Meta-stable O_2^{2-} peroxide defect formation in AOS by NBIS or IS has been recently proposed.[32] With excited holes in the valence band tail (VBT) states in AOS, the empty $pp\sigma^*$-like VBT states induce a driving force to form an O-O bond through the $pp\sigma$ bonding interaction. Along with the O-O bond formation, the $pp\sigma^*$ state is heightened up into the CBs, and the electrons excited are doped with occupying the conduction band minimum (CBM) state. The energy barrier from the meta-stable O_2^{2-} peroxide to the normal amorphous oxide configuration is 0.97 eV in the hybrid density-functional theory (DFT) calculations.[32]

In order to improve the stability of AOS-based TFTs against the bias and illumination stresses, a variety of attempts, such as a novel TFT architecture (including adopting a passivation layer),[5,23,33,34] changing the gate insulator material,[4,24] process design (for examples, O_2 or water annealing),[21,24,35] impurity doping in AOS,[2] and optimizing the cation species and compositions of the AOS materials,[26,36] have been made. The improvement of stability should not accompany (or at least minimize) any degradation of the electron mobility in the AOS. In this study, we investigate the cation composition effects on the electronic structures of In-Sn-Zn-O amorphous semiconductors to optimize both the stability and the mobility. We find that the CBM and VBT show nearly monotonic changes with respect to the In and Sn cation composition ratios. The In-5*s* and Sn-5*s* orbital overlaps and the stronger O-O $pp\sigma^*$ orbital coupling near the In and Sn atoms are found to be responsible for the CBM and VBT changes, respectively. The results indicate that the electron mobility and the stability are in a trade-off relation, when they are controlled by the In and Sn contents in amorphous In-Sn-Zn-O.

II. METHODS

We performed DFT calculations as implemented in the Vienna *ab initio* simulation package (VASP) code.[37,38] The projector-augmented wave pseudopotentials[39] and the plane-wave basis set with a kinetic energy cutoff of 400 eV were used. The local-density approximation[40] plus U (LDA+U)[41] was used for the exchange correlation energy with the on-site Coulomb energy U of 6 eV for the In, Ga, and Zn d states. The Sn 4d were treated as core states. For the Brillouin zone integration in DFT molecular dynamics simulations, a single k-point at (0.25, 0.25, 0.25) was used. The total energy difference between the single k-point and the $2 \times 2 \times 2$ Monkhorst-Pack mesh is only a few meV. In electronic density-of-states calculations, we used the $3 \times 3 \times 3$ mesh including the Γ k-point. The LDA+U method with $U = 6$ eV was tested for crystalline ZnO. The major role of U for the Zn-3d states in ZnO is correction of the energy level position of the Zn-3d bands.[42] The Zn-3d bands are located near −7 eV below the valence band maximum (VBM) in our LDA + U calculations, and is close to the X-ray emission spectroscopy measurements.[43] With this correction, the band gap underestimation problem of the LDA is partially improved by suppressing the spurious Zn-3d and O-2p hybridization in the LDA. The calculated LDA + U band gap of ZnO was 1.74 eV, while the LDA band gap was 0.80 eV. The calculated LDA and LDA + U gaps are consistent with the previous LDA + U calculations,[44] but still lower than the experimental,[45] hybrid functional,[46,47] and GW[48–53] results. Thus, here we focus only on the *changes* of the band gaps with respect to the cation compositions.

The considered metal compositions of the In-Sn-Zn-O amorphous semiconductors are listed in Table I. We used cubic supercells. The number of atoms for each atom species (N_{In}, N_{Sn}, N_{Zn}, and N_O) and the total number of atoms (N_t) in the supercell are shown in Table I. We only considered O stoichiometric condition as in the binary oxides of In_2O_3, SnO_2, and ZnO. The supercell volumes (V_t) are derived from the experimental mass densities of In_2O_3 (7180 kg/m^3), SnO_2 (6900 kg/m^3), and ZnO (5600 kg/m^3). We also considered amorphous $InGaZnO_4$ as a reference AOS. The number of atoms in the $InGaZnO_4$ cubic supercell is $N_t = 168$ with $N_{In} = 24$, $N_{Ga} = 24$, $N_{Zn} = 24$, and $N_O = 96$. The $InGaZnO_4$ supercell volume is also derived from the experimental mass densities [Ga_2O_3 (6000 kg/m^3)] ($V_t = 1972.9$ Å^3). The average volume per unit formula obtained by this *a priori* approach for the amorphous phase $InGaZnO_4$ is 9.6% larger than the theoretically optimized volume per unit formula for the crystalline phase $InGaZnO_4$. The amorphous structures were generated by melt-and-quenching molecular dynamics simulations within the Nosé canonical ensemble. A random amorphous oxide structure was melted at 3000 K for 6 ps and then quenched down to 300 K at a quenching rate of 900 K/ps. The amorphous structure was then optimized with the static DFT calculations until the Hellmann-Feynman forces were less than 0.02 eV/Å.

TABLE I. Seven considered amorphous In-Sn-Zn-O semiconductors in this work are listed. N_{In}, N_{Sn}, N_{Zn}, and N_O are the numbers of In, Sn, Zn, and O atoms, respectively, in the supercell. N_t is the total number of atoms in the supercell, and V_t is the total supercell volume. $R_{In}+R_{Sn}$ is the sum of the In and Sn composition ratios.

Sample	N_{In}	N_{Sn}	N_{Zn}	N_O	N_t	V_t (Å^3)	$R_{In}+R_{Sn}$
ISZO#1	24	24	24	108	180	2221.0	0.667
ISZO#2	12	24	24	90	150	1835.6	0.600
ISZO#3	6	27	27	90	150	1824.2	0.550
ISZO#4	10	16	24	71	121	1481.1	0.520
ISZO#5	6	8	16	41	71	869.2	0.467
ISZO#6	10	12	28	67	117	1432.5	0.440
ISZO#7	6	18	36	81	151	1714.9	0.400

Downloaded 29 Aug 2013 to 210.123.42.185. This article is copyrighted as indicated in the abstract. Reuse of AIP content is subject to the terms at: http://jap.aip.org/about/rights_and_permissions

The limited number of atoms with the supercell structures and the melt-and-quenching simulation method to generate the amorphous structures can restrict accurate description of the experimentally obtained amorphous structures (typically by sputtering and annealing). Nevertheless, such a structural modeling has been widely accepted in previous DFT studies and explained the experimental results such as extended X-ray absorption fine structures (EXAFS).[54] We could also reproduce the well known trade-off relation between the mobility and stability of AOS, and its chemical origins are focused on here.

III. RESULTS

A. Trends

The calculated electronic densities of states (DOS) in LDA+U for the considered In-Sn-Zn-O amorphous semiconductors are shown in Fig. 1. We aligned the energy levels by comparing the In-4d levels of the In-Sn-Zn-O with those of the crystalline $InGaZnO_4$. Minimizing the absolute value of the difference of the In-4d partial DOS between the amorphous In-Sn-Zn-O and the crystalline $InGaZnO_4$ is found to yield a good alignment of the energy levels, as shown in Fig. 1(a). We can see the overall agreements of the deep O-2s, In-4d, Zn-3d, and O-2p states in level positions between the difference compositions. The zero energy level is set to the top-most valence band state level of the crystalline $InGaZnO_4$. Near the valence and conduction band edges, the changes of the VBT extents in energy level and the CBM levels are found, as shown in Fig. 1(b).

We plot the top-most VBT levels, the CBM levels, and their differences (the fundamental LDA+U energy gaps) as a function of the sum of the In and Sn ratios ($R_{In}+R_{Sn}$) in Fig. 2(a). We define here the composition ratio of a metal

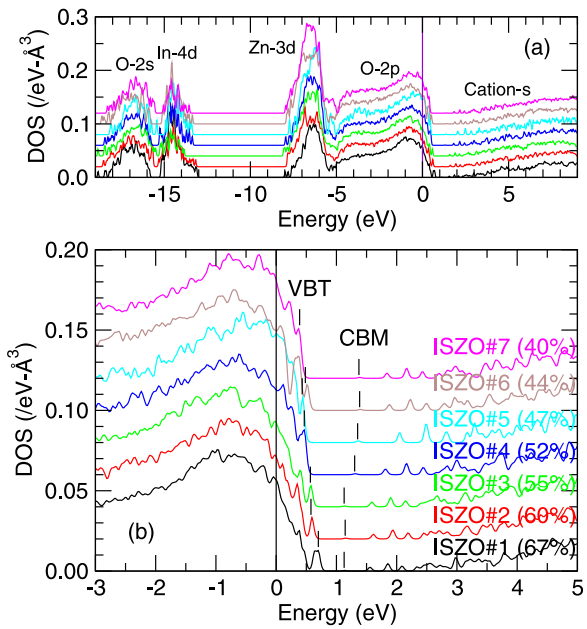

FIG. 1. Calculated total electronic densities of states for the considered In-Sn-Zn-O samples (a) in a wide range of the energy level and (b) near the valence and conduction band edges. With decreasing the sum of the In and Sn ratios from the ISZO#1, the density of states is shifted by $+0.02\,eV^{-1}Å^{-3}$.

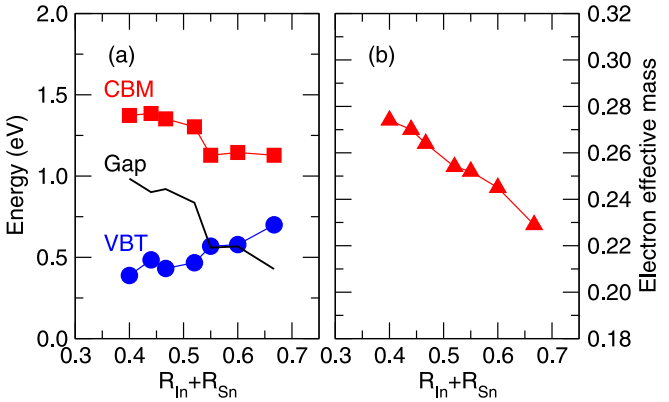

FIG. 2. (a) Calculated top-most VBT levels (filled circles), CBM levels (filled rectangles), and energy gaps (solid line) in LDA+U are plotted as a function of the sum of the In and Sn ratios ($R_{In}+R_{Sn}$). (b) Calculated electron effective masses (filled triangles) are plotted as a function of the $R_{In}+R_{Sn}$.

cation as $R_M = N_M/(N_{In}+N_{Sn}+N_{Zn})$, where M is one of the In, Sn, and Zn. It is found that the levels show almost monotonic changes with respect to the $R_{In}+R_{Sn}$ ratio. We could not find any such correlations of the energy levels with the other parameters, for example, with the In ratio (R_{In}) nor with the Sn ratio (R_{Sn}), while necessarily there are correlations with the Zn ratio [$R_{Zn} = 1-(R_{In}+R_{Sn})$]. The CBM level is found to be lowered, the top-most VBT level is raised, and the band gap is correspondingly narrowed, as the $R_{In}+R_{Sn}$ ratio increases. Although the LDA+U exchange correlation energy in DFT is well known to underestimate the band gaps severely, here we are only interested in the changes of the band edge levels with respect to the cation compositions and their chemical origins, qualitatively. Figure 2(b) shows the calculated electron effective masses (m_e^*) of the In-Sn-Zn-O's. The m_e^* shows a monotonic decrease as the $R_{In}+R_{Sn}$ ratio increases.

B. Conduction band minimum

The CBM level lowering as the $R_{In}+R_{Sn}$ ratio increases can be understood from the cation metal s-orbital overlaps. In Fig. 3(a), the calculated portions of the s-projected CBM density of states for the In-5s, Sn-5s, Zn-4s, and O-2s are shown. The CBM states of the In-Sn-Zn-O's are found to

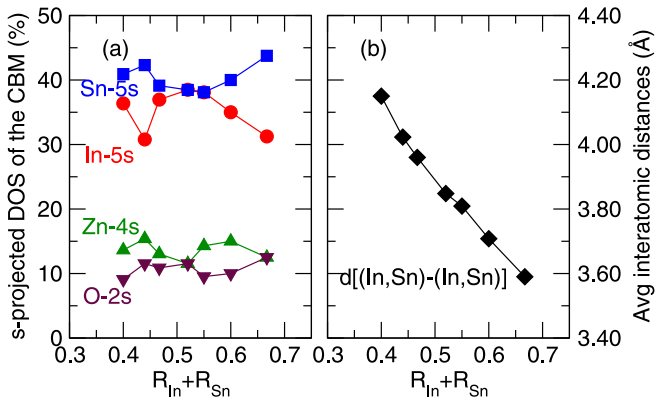

FIG. 3. Calculated (a) atomic-orbital portions (s-orbital projected DOS) of the CBM state and (b) average inter-atomic distances between the In and Sn atoms, as a function of the $R_{In}+R_{Sn}$ ratio in amorphous In-Sn-Zn-O.

Downloaded 29 Aug 2013 to 210.123.42.185. This article is copyrighted as indicated in the abstract. Reuse of AIP content is subject to the terms at: http://jap.aip.org/about/rights_and_permissions

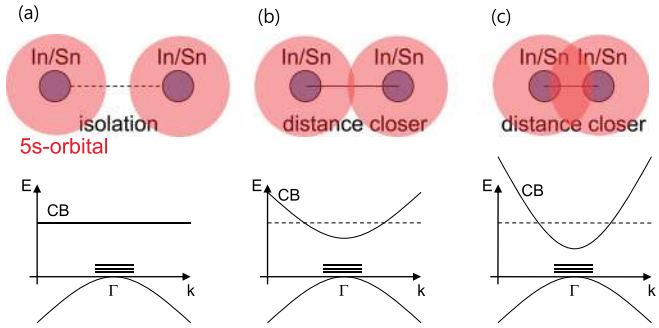

FIG. 4. Schematic diagram showing the In and Sn 5*s* orbital overlaps and the conduction band dispersions, when (a) the cations are isolated, (b) the inter-distances between the In and Sn atoms are closer, and (c) the inter-distances are furthermore closer.

mainly consist of the In-5*s* and Sn-5*s* atomic orbital states. The Sn-5*s* character is found to be slightly stronger than the In-5*s* for the CBM in some metal compositions, and the sum of the In-5*s* and Sn-5*s* portions is approximately as high as 80%, irrespective of the metal compositions. Both the In-5*s* and Sn-5*s* orbitals with similar contributions form the main channel of the electron conduction in amorphous In-Sn-Zn-O.

On the other hand, the effective inter-atomic distances between the In and Sn atoms in In-Sn-Zn-O are changed depending on the cation compositions. As shown in Fig. 3(b), the average inter-atomic distances between the In and Sn atoms are closer as the $R_{In}+R_{Sn}$ ratio increases. The average inter-atomic distance between the In atoms in $InGaZnO_4$ is 4.35 Å, of which the R_{In} ratio is 33%. The average inter-atomic distance between the In and Sn atoms becomes closer down to 3.59 Å, when the $R_{In}+R_{Sn}$ is 67% in In-Sn-Zn-O, as shown in Fig. 3(b).

It can be easily expected that the closer inter-atomic distances between In and Sn atoms should make the overlaps between the In-5*s* and Sn-5*s* atomic orbitals more effective in amorphous In-Sn-Zn-O. As the In and Sn density increases, the increased overlaps of the In-5*s* and Sn-5*s* orbitals extend the conduction band dispersion, as schematically shown in Fig. 4. Accordingly, the CBM level is lowered [Fig. 2(a)], and the electron effective mass is reduced [Fig. 2(b)], as the $R_{In}+R_{Sn}$ ratio increases.

C. Valence band tail

The understanding of the CBM changes with respect to the $R_{In}+R_{Sn}$ ratio in In-Sn-Zn-O is rather straightforward through the conducting channels made of the In and Sn 5*s* orbitals. However, the change of the VBT extent depending on the $R_{In}+R_{Sn}$ ratio [Fig. 2(a)] is not simply as expected, because the VBT states are thought to be mostly O-related and barely related to the cation compositions.

The orbital character of the VBT states is mostly O-2*p* in the ionic-bonded material. The upper part of the valence O-2*p* bands consists of the O-2*p* anti-bonding states, while the lower part of the bands consists of the O-2*p* bonding states. In Fig. 5, we schematically draw the valence O-2*p* bands comprising the various O-2*p* orbital states. In crystalline oxides [Fig. 5(a)], the crystal field split levels of the O-2*p* atomic orbital states are well degenerated in inter-sites by the structural order, and by the inter-site *p-p* orbital coupling, the valence O-2*p* bands are delocalized. The lower part of the bands is the $pp\sigma$ and $pp\pi$ mixed bonding states, and the upper part is the $pp\sigma^*$ and $pp\pi^*$ mixed anti-bonding states. We find that the top-most valence band state of the crystalline $InGaZnO_4$ is mostly the delocalized $pp\sigma^*$ and $pp\pi^*$ mixed anti-bonding state [see Fig. 6(a)].

One of the main differences in valence O-2*p* bands between the amorphous and crystalline oxides is the existence of the VBT states, which is the highest among the valence O-2*p* states [see Fig. 5(b)]. Among the inter-site *p-p* orbital coupling, the $pp\sigma^*$ is the highest in energy level, and then the VBT states in amorphous oxides should have at least partly the character of the O-O $pp\sigma^*$ orbitals. In disordered amorphous structure, the crystal field splitting of the atomic O-2*p* orbitals is complex, and the high energy O-2*p* orbitals will contribute to the VBT states more strongly [indicated by the high energy *p* orbital levels in Fig. 5(b)]. We plot the calculated charge densities of the top-most VBT states for the considered seven amorphous In-Sn-Zn-O compositions [Figs. 6(b)–6(h)] and the amorphous $InGaZnO_4$ [Fig. 6(i)]. For the amorphous oxides, all show the O-O $pp\sigma^*$ orbitals in the VBT states clearly. For amorphous $InGaZnO_4$, the $pp\sigma^*$ character of the VBT state is also seen in other works.[55,56]

We find a slight overlap of the Zn-3*d* and O-2*p* bands in DOS of the amorphous oxides [see Fig. 1(a)]. By the *p-d*

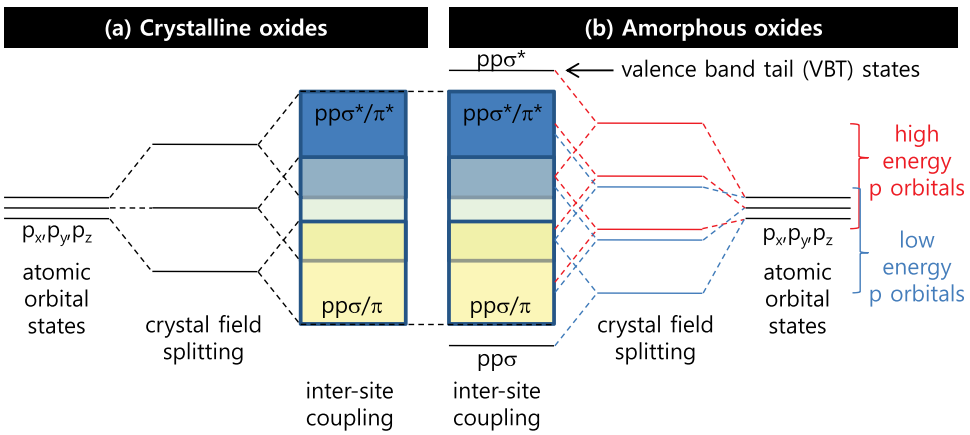

FIG. 5. Schematic diagram of the valence O-2*p* bands in (a) crystalline and (b) amorphous oxides. The lower part of the bands is $pp\sigma$ and $pp\pi$ bonding states, while the upper part is $pp\sigma^*$ and $pp\pi^*$ anti-bonding. In amorphous oxides, the highest level is the $pp\sigma^*$ anti-bonding state resulting from the high energy *p* orbitals in the disordered structure.

Downloaded 29 Aug 2013 to 210.123.42.185. This article is copyrighted as indicated in the abstract. Reuse of AIP content is subject to the terms at: http://jap.aip.org/about/rights_and_permissions

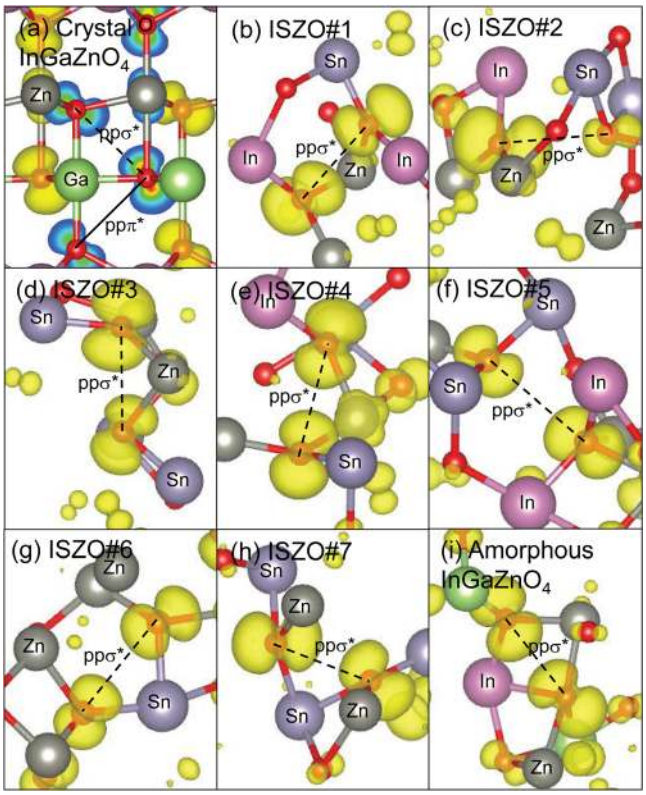

FIG. 6. Calculated charge densities of (a) the top-most valence state of the crystalline $InGaZnO_4$, [(b)-(i)] the top-most VBT state of the amorphous In-Sn-Zn-O [(b)–(h)], and amorphous $InGaZnO_4$ (i). The dashed lines connect two O atoms that have the $pp\sigma^*$ orbital in the VBT state. The solid line in (a) indicates the $pp\pi^*$ orbital ordering.

hybridization, a small contribution of the Zn-3*d* states in VBT can be induced, which can be seen in Fig. 6(e), as previously reported.[55] However, the Zn-3*d* contribution to the VBT states is found to be weaker than the O-O $pp\sigma^*$, as seen in the charge densities shown in Fig. 6.

Then, why is the O inter-site $pp\sigma^*$-related VBT level extent affected by the $R_{In}+R_{Sn}$ ratio in amorphous In-Sn-Zn-O? We first investigate the O-O inter-distances in the amorphous In-Sn-Zn-O, because, when the O-O inter-distance is closer, the O-O inter-site coupling ($pp\sigma$-$pp\sigma^*$) can be stronger. Figure 7 shows the calculated radial pair-distribution functions (*r*PDF) of O-O for the amorphous In-Sn-Zn-O and $InGaZnO_4$. The nearest neighbor O-O distances are found in the range of 2.5-3.5 Å, and we could not find a significant reduction of the O-O distances for the amorphous In-Sn-Zn-O having a high $R_{In}+R_{Sn}$ ratio. All the calculated amorphous oxides have a similar O-O distance distributions, as shown in Fig. 7. Therefore, the VBT extent increase with the $R_{In}+R_{Sn}$ ratio cannot be attributed to the O-O inter-distance shortening.

The O-2*p* orbital directions are various in amorphous oxides by the orientational disorder of the amorphous structure, which is, in fact, the origin of the *p* orbital localization and the VBT states. Among the various O-2*p* orbitals, the O-2*p* directed along the *M*-O bond is electrostatically stable, since the *M* cation atoms attract electrons, and their electronic energy levels are relatively deep in the valence O-2*p* bands [low energy *p* orbitals, indicated in Fig. 5(b)]. On the

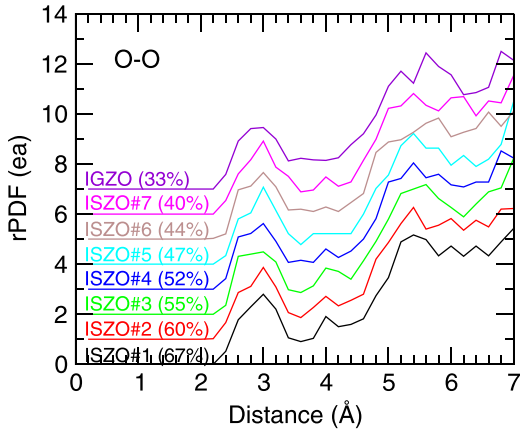

FIG. 7. Calculated *r*PDF between O atoms for amorphous In-Sn-Zn-O and $InGaZnO_4$. In the parenthesis, the $R_{In}+R_{Sn}$ ratios are indicated. With decreasing the $R_{In}+R_{Sn}$ ratio from the ISZO#1 (67%), the *r*PDF is shifted by +1 ea.

other hand, the O-2*p* orbital directed off the *M*-O bonds is high in electrostatic energy, and forms a higher energy level in the valence O-2*p* bands [high energy *p* orbitals, indicated in Fig. 5(b)]. By coupling of the off-bond O-2*p* orbital with a nearby O-2*p* orbital, the probability of forming the VBT states becomes high. Therefore, the inter-site coupling between the off-bond O-2*p* orbitals can be important for the VBT characterization.

In the case of the inter-site coupling between two off-bond O-2*p* orbitals, the O-*M*-O bond angles can be important in amorphous oxides. As the O-*M*-O bond angle is smaller, the inter-site $pp\sigma^*$ coupling of the off-bond O-2*p* orbitals can be stronger (Fig. 8), and especially when the O-*M*-O bond angle is acute smaller than 90°, the $pp\sigma^*$ coupling can be significantly enhanced, as shown in Fig. 8(c). It is worthwhile to mention the preferred coordination numbers of In, Sn, and Zn cations in oxides. The In and Sn atoms preferentially form octahedral configuration with bonding to nearby 6 O atoms (6-fold coordination) [Figs. 9(c) and 9(d)], while the Zn atoms preferentially form tetrahedral configuration with 4 nearby O atoms (4-fold coordination) [Fig. 9(a)]. The Ga atoms are known to have a preferentially 5-fold coordination number [Fig. 9(b)]. Especially, for the octahedral configuration with the nearby 6 O atoms, the O-*M*-O angles are 90° in a crystal and can be acute more probably in amorphous structure.

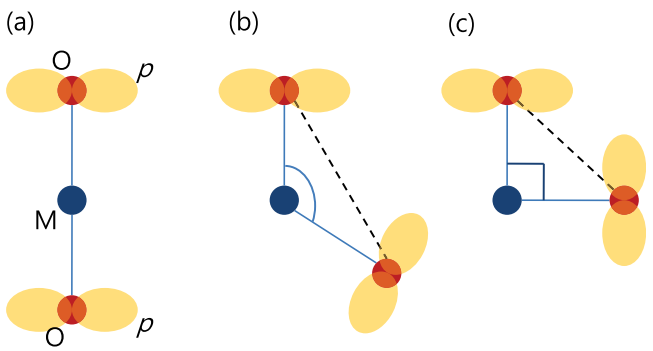

FIG. 8. Schematic diagrams showing the inter-site coupling between two high-energy (off-bond) O-2*p* orbitals, which depends on the O-M-O angles: (a) 180°, (b) ~120°, and (c) 90°.

Downloaded 29 Aug 2013 to 210.123.42.185. This article is copyrighted as indicated in the abstract. Reuse of AIP content is subject to the terms at: http://jap.aip.org/about/rights_and_permissions

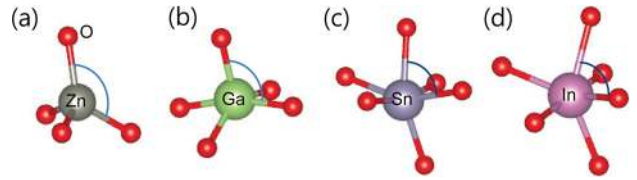

FIG. 9. Local atomic configurations near a (a) Zn, (b) Ga, (c) Sn, and (d) In in amorphous ISZO#1 and amorphous $InGaZnO_4$.

We investigated the O-*M*-O bond angle distributions for the amorphous In-Sn-Zn-O and $InGaZnO_4$, as shown in Figs. 10(a)–10(h). For In and Sn atoms, the number of O-*M*-O angles [$M = $(In, Sn)] are abundant in the range of 70°-90°, and there is a small peak near 140°-180°, which indicates the octahedral configuration of InO_6 and SnO_6 [see Figs. 9(c) and 9(d)]. On the other hand, near Zn atoms, the largest amount of O-*M*-O angles ($M = $Zn) are found in the range of 80°–120°. The O-Zn-O bond angles are larger than the small O-(In, Sn)-O bond angles. For amorphous $InGaZnO_4$, the number of O-Ga-O bond angles is the most in the range of 80°-110° [Fig. 10(h)]. Although the O-O distances in the amorphous oxides do not show a significant difference between the different cation compositions (as shown in Fig. 7), the O-*M*-O bond angles show a clear difference depending on the metal cation species, *M*. That is because the In-O (~2.1 Å) and Sn-O (~2.1 Å) bond lengths are larger than the Zn-O (~1.9 Å) bond length, and thus even with the smaller O-*M*-O bond angles, the O-O distances keep a value in the range of 2.5-3.5 Å (see Fig. 7), irrespective of the nearby *M* cations in the amorphous oxides.

The densities of acute O-*M*-O bond angles are plotted as a function of the $R_{In}+R_{Sn}$ ratio in Fig. 10(i). They are found to increase as the $R_{In}+R_{Sn}$ ratio increases in the amorphous oxides. When In and Sn contents are increased in amorphous In-Sn-Zn-O, a large number of acute O-*M*-O angles will appear, and they make the O-O $pp\sigma$-$pp\sigma^*$ coupling between two off-bond O-2*p* orbitals stronger. That is, although the VBT states are mostly characterized by the O-2*p* orbitals, they are affected by the metal cation compositions. The O atoms near the In and Sn cations are more strongly interacting and have a higher probability of forming the $pp\sigma^*$ hybridized orbital states in the VBT in amorphous In-Sn-Zn-O.

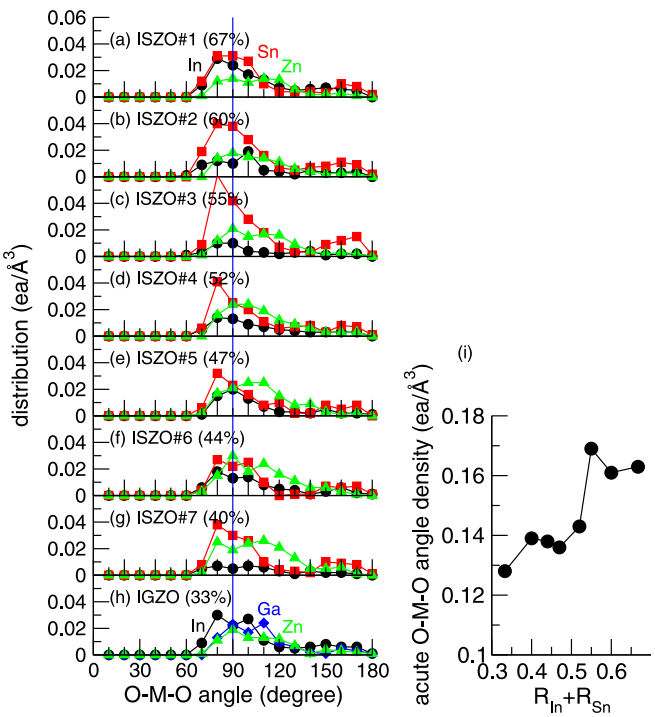

FIG. 10. (a)–(h) O-*M*-O bond angle distributions for the amorphous In-Sn-Zn-O and amorphous $InGaZnO_4$. The *M* is for In (circle), Sn (square), Zn (triangle), and Ga (diamond). (i) Volumetric densities of the acute O-*M*-O bond angles (≤90°) in the amorphous oxides, as a function of the $R_{In}+R_{Sn}$ ratio.

As the $R_{In}+R_{Sn}$ ratio increases, the R_{Zn} ratio decreases correspondingly. In our results, as the R_{Zn} ratio decreases, the VBT level extent increases. If we considered the partial contribution of the Zn-3*d* states in the VBT states, the trend should be opposite. However, it is not the case, because as the R_{Zn} ratio increases, only the Zn-3*d* peak intensity in the total DOS is heightened [as shown in Fig. 1(a)], whereas the Zn-3d band dispersion is little changed. For the *p*-*d* hybridization strength, the band overlap between the Zn-3*d* and O-2*p* states is more influential than the density of the Zn-3*d* states. Thus, the VBT level extent changes with the cation compositions are not considered to be related to the Zn-3*d* states.

IV. DISCUSSION

Recently, it has been proposed that the NBIS and IS instabilities of AOS-based TFTs are partially attributed to the VBT holes generated by the negative gate bias and/or illumination stress.[32] We showed that the VBT states in AOS are characterized by the $pp\sigma^*$ electronic orbitals, in Sec. III C. The empty $pp\sigma^*$-like VBT states by the excited holes can generate a driving force to form an O-O bond by the $pp\sigma$ bonding interaction, resulting in the O_2^{2-} peroxide defect formation. The O_2^{2-} peroxide defect is previously found to be a meta-stable donor defect.[32] Therefore, the increased VBT extents in the In- and Sn-rich AOS can worsen the hole-induced (NBIS and IS) instabilities of the AOS, even though the electron mobility can be enhanced by the increased densities of In and Sn. On the other hand, the V_O's in AOS have been also proposed as an origin to give the NBIS instability in AOS-based TFTs.[19–22,24,30,31] Since the In-O and Sn-O bonds are weaker than the Ga-O and Zn-O bonds, the V_O formation can be enhanced with the increased densities of In and Sn, which can worsen again but as a different mechanism the NBIS and IS instabilities of the AOS. Therefore, we can expect that the electron mobility and stability of AOS can be in a trade-off relation, when they are controlled by the In and Sn compositions in AOS.

V. CONCLUSION

Based on DFT calculations, the effects of cation compositions on the electronic structures of amorphous In-Sn-Zn-O semiconductors were investigated. We found that the CBM energy level and the electron effective mass (m_e^*) decrease with the sum of In and Sn composition ratios ($R_{In}+R_{Sn}$). The electron carrier mobility can be increased with increasing the In and Sn contents in amorphous In-Sn-Zn-O by reducing the effective mass. However, as the sum of In and

Downloaded 29 Aug 2013 to 210.123.42.185. This article is copyrighted as indicated in the abstract. Reuse of AIP content is subject to the terms at: http://jap.aip.org/about/rights_and_permissions

Sn ratios increases, the VBT is found to be extended, which can worsen the stability of the AOS-based TFTs.[32] The VBT extent is found to be due to the increased density of In and Sn cations, near which the O-2*p* inter-site $pp\sigma^*$ coupling is stronger than that near the Zn atoms. The acute O-(In,Sn)-O angle is suggested to be an important local structural parameter in amorphous oxide semiconductors, which renders the O-O $pp\sigma^*$ coupling more effective. The electron mobility and the stability are thus in a trade-off relation, when they are controlled by the In and Sn contents in amorphous In-Sn-Zn-O.

ACKNOWLEDGMENTS

This research was supported by Nano R&D program through the National Research Foundation (NRF) of Korea funded by the Ministry of Education, Science, and Technology (MEST) (No. 2012-0006199).

[1]K. Nomura, H. Ohta, A. Takagi, T. Kamiya, M. Hirano, and H. Hosono, Nature **432**, 488 (2004).
[2]B. S. Yang, M. S. Huh, S. Oh, U. S. Lee, Y. J. Kim, M. S. Oh, J. K. Jeong, C. S. Hwang, and H. J. Kim, Appl. Phys. Lett. **98**, 122110 (2011).
[3]J.-S. Park, K. Kim, Y.-G. Park, Y.-G. Mo, H. D. Kim, and J. K. Jeong, Adv. Mater. **21**, 329 (2009).
[4]J.-Y. Kwon, J. S. Jung, K. S. Son, K.-H. Lee, J. S. Park, T. S. Kim, J.-S. Park, R. Choi, J. K. Jeong, B. Koo, and S. Y. Lee, Appl. Phys. Lett. **97**, 183503 (2010).
[5]S. Yang, D.-H. Cho, M. K. Ryu, S.-H. K. Park, C.-S. Hwang, J. Jang, and J. K. Jeong, Appl. Phys. Lett. **96**, 213511 (2010).
[6]I. J. Kang, C. H. Park, E. Chong, and S. Y. Lee, Curr. Appl. Phys. **12**, S12 (2012).
[7]J. Robertson, J. Non-Cryst. Solids **354**, 2791 (2008).
[8]K. Nomura, A. Takagi, T. Kamiya, H. Ohta, M. Hirano, and H. Hosono, Jpn. J. Appl. Phys., Part 1 **45**, 4303 (2006).
[9]Y. Sun and J. A. Rogers, Adv. Mater. **19**, 1897 (2007).
[10]H. Yabuta, M. Sano, K. Abe, T. Aiba, T. Den, H. Kumomi, K. Nomura, T. Kamiya, and H. Hosono, Appl. Phys. Lett. **89**, 112123 (2006).
[11]P. Görrn, H. Hölzer, W. Kowalsky, J. Wang, T. Weimann, P. Hinze, and S. Kipp, Appl. Phys. Lett. **90**, 063502 (2007).
[12]A. Suresh and J. F. Muth, Appl. Phys. Lett. **92**, 033502 (2008).
[13]J.-M. Lee, I.-T. Cho, J.-H. Lee, and H.-I. Kwon, Appl. Phys. Lett. **93**, 093504 (2008).
[14]M. E. Lopes, H. L. Gomes, M. C. R. Medeiros, P. Barquinha, L. Pereira, E. Fortunato, R. Martins, and I. Ferreira, Appl. Phys. Lett. **95**, 063502 (2009).
[15]J. K. Jeong, H. W. Yang, J. H. Jeong, Y.-G. Mo, and H. D. Kim, Appl. Phys. Lett. **93**, 123508 (2008).
[16]K. Nomura, T. Kamiya, M. Hirano, and H. Hosono, Appl. Phys. Lett. **95**, 013502 (2009).
[17]W.-T. Chen, H.-W. Hsueh, H.-W. Zan, and C.-C. Tasi, Electrochem. Solid-State Lett. **14**, H297 (2011).
[18]J.-H. Shin, J.-S. Lee, C.-S. Hwang, S.-H. K. Park, W. S. Cheong, M. Ryu, C.-W. Byun, J.-I. Lee, and H. Y. Chu, ETRI J. **31**, 62 (2009).
[19]H. Oh, S.-M. Yoon, M. K. Ryu, C.-S. Hwang, S. Yang, and S.-H. K. Park, Appl. Phys. Lett. **97**, 183502 (2010).
[20]M. D. H. Chowdhury, P. Migliorato, and J. Jang, Appl. Phys. Lett. **97**, 173506 (2010).
[21]K. H. Ji, J.-I. Kim, H. Y. Jung, S. Y. Park, R. Choi, U. K. Kim, C. S. Hwang, D. Lee, H. Hwang, and J. K. Jeong, Appl. Phys. Lett. **98**, 103509 (2011).
[22]H. Oh, S.-M. Yoon, M. K. Ryu, C.-S. Hwang, S. Yang, and S.-H. K. Park, Appl. Phys. Lett. **98**, 033504 (2011).
[23]H. Oh, S.-H. K. Park, C.-S. Hwang S. Yang, and M. K. Ryu, Appl. Phys. Lett. **99**, 022105 (2011).
[24]K. H. Ji, J.-I. Kim, H. Y. Jung, S. Y. Park, R. Choi, Y. G. Mo, and J. K. Jeong, Microelectron. Eng. **88**, 1412 (2011).
[25]P. Barquinha, A. Pimentel, A. Marques, L. Pereira, R. Martins, and E. Fortunato, J. Non-Cryst. Solids **352**, 1756 (2006).
[26]P. Görrn, M. Lehnhardt, T. Riedl, and W. Kowalsky, Appl. Phys. Lett. **91**, 193504 (2007).
[27]C.-S. Chuang, T.-C. Fung, B. G. Mullins, K. Nomura, T. Kamiya, H.-P. D. Shieh, H. Hosono, and J. Kanicki, Proc. Soc. Inf. Display **39**, 1215 (2008).
[28]D. P. Gosain and T. Tanaka, Jpn. J. Appl. Phys., Part 1 **48**, 03B018 (2009).
[29]D. H. Lee, K. Kawamura, K. Nomura, T. Kamiya, and H. Hosono, Electrochem. Solid-State Lett. **13**, H324 (2010).
[30]B. Ryu, H.-K. Noh, E.-A. Choi, and K. J. Chang, Appl. Phys. Lett. **97**, 022108 (2010).
[31]H.-K. Noh, K. J. Chang, B. Ryu, and W.-J. Lee, Phys. Rev. B **84**, 115205 (2011).
[32]H.-H. Nahm, Y.-S. Kim, and D. H. Kim, Phys. Status Solidi B **249**, 1277 (2012).
[33]M. Kim, J. H. Jeong, H. J. Lee, T. K. Ahn, H. S. Shin, J.-S. Park, J. K. Jeong, Y.-G. Mo, and H. D. Kim, Appl. Phys. Lett. **90**, 212114 (2007).
[34]J. S. Park, T. S. Kim, K. S. Son, K.-H. Lee, W.-J. Maeng, H.-S. Kim, E. S. Kim, K.-B. Park, J.-B. Seon, W. Choi, M. K. Ryu, and S. Y. Lee, Appl. Phys. Lett. **96**, 262109 (2010).
[35]J. S. Park, T. S. Kim, K. S. Son, W.-J. Maeng, H.-S. Kim, M. Ryu, and S. Y. Lee, Appl. Phys. Lett. **98**, 012107 (2011).
[36]T. Riedl, P. Görrn, H. Hölzer, and W. Kowalsky, Phys. Status Solidi (RRL) **1**, 175 (2007).
[37]G. Kresse and J. Furthmüller, Phys. Rev. B **54**, 11169 (1996).
[38]G. Kresse and D. Joubert, Phys. Rev. B **59**, 1758 (1999).
[39]P. E. Blöchl, Phys. Rev. B **50**, 17953 (1994).
[40]D. M. Ceperley and B. J. Alder, Phys. Rev. Lett. **45**, 566 (1980).
[41]V. I. Anisimov, I. V. Solovyev, M. A. Korotin, M. T. Czyżyk, and G. A. Sawatzky, Phys. Rev. B **48**, 16929 (1993).
[42]W.-J. Lee and Y.-S. Kim, J. Korean Phys. Soc. **60**, 781 (2012).
[43]C. L. Dong, C. Persson, L. Vayssieres, A. Augustsson, T. Schmitt, M. Mattesini, R. Ahuja, C. L. Chang, and J.-H. Guo, Phys. Rev. B **70**, 195325 (2004).
[44]A. Janotti, D. Segev, and C. G. Van de Walle, Phys. Rev. B **74**, 045202 (2006).
[45]J. E. Jaffe and A. C. Hess, Phys. Rev. B **48**, 7903 (1993).
[46]F. Oba, A. Togo, I. Tanaka, J. Paier, and G. Kresse, Phys. Rev. B **77**, 245202 (2008).
[47]S. J. Clark, J. Robertson, S. Lany, and A. Zunger, Phys. Rev. B **81**, 115311 (2010).
[48]S. Massidda, R. Resta, M. Posternak, and A. Baldereschi, Phys. Rev. B **52**, R16977 (1995).
[49]M. Shishkin and G. Kresse, Phys. Rev. B **75**, 235102 (2007).
[50]M. Shishkin, M. Marsman, and G. Kresse, Phys. Rev. Lett. **99**, 246403 (2007).
[51]F. Fuchs, J. Furthmüller, F. Bechstedt, M. Shishkin, and G. Kresse, Phys. Rev. B **76**, 115109 (2007).
[52]B.-C. Shih, Y. Xue, P. Zhang, M. L. Cohen, and S. G. Louie, Phys. Rev. Lett. **105**, 146401 (2010).
[53]M. Stankovski, G. Antonius, D. Waroquiers, A. Miglio, H. Dixit, K. Sankaran, M. Giantomassi, X. Gonze, M. Cóte, and G.-M. Rignanese, Phys. Rev. B **84**, 241201(R) (2011).
[54]K. Nomura, T. Kamiya, H. Ohta, T. Uruga, M. Hirano, and H. Hosono, Phys. Rev. B **75**, 035212 (2007).
[55]A. Walsh, J. L. F. Da Silva, and S.-H. Wei, Chem. Mater. **21**, 5119 (2009).
[56]T. Kamiya, K. Nomura, and H. Hosono, J. Disp. Technol. **5**, 273 (2009).

Downloaded 29 Aug 2013 to 210.123.42.185. This article is copyrighted as indicated in the abstract. Reuse of AIP content is subject to the terms at: http://jap.aip.org/about/rights_and_permissions